Electron count and ligand composition influence the optical and chiroptical signatures of far-red and NIR-emissive DNA-stabilized silver nanoclusters

Rweetuparna Guha,^a Anna Gonzàlez-Rosell,^a Malak Rafik,^a Nery Arevalos,^a Benjamin B. Katz,^b Stacy M. Copp, ^{a,c,d*}

Abstract: Near-infrared (NIR) emissive DNA-stabilized silver nanoclusters (Agn-DNAs) are promising fluorophores in the biological tissue transparency windows. Hundreds of NIR-emissive Agn-DNAs have recently been discovered, but their structure-property relationships remain poorly understood. Here, we investigate 19 different far-red and NIR emissive Agn-DNA species stabilized by 10-base DNA templates, including well-studied emitters whose compositions and chiroptical properties have never been reported before. The molecular formula of each purified species is determined by high-resolution mass spectrometry and correlated to its optical absorbance, emission, and circular dichroism (CD) spectra. We find that there are four distinct compositions for Agn-DNAs emissive at the far red/NIR spectral border. These emitters are either 8-electron clusters stabilized by two DNA oligomer copies or 6-electron clusters with one of three different ligand compositions: two oligomer copies, three oligomer copies, or two oligomer copies with additional chlorido ligands. Distinct optical and chiroptical signatures of 6-electron Agn-DNAs correlate with each ligand composition. Agn-DNAs with three oligomer ligands exhibit shorter Stokes shifts than Agn-DNAs with two oligomers, and Agn-DNAs with chlorido ligands

^a Department of Materials Science and Engineering, University of California, Irvine, CA 92697, USA

^b Department of Chemistry, University of California, Irvine, CA 92697, USA

^c Department of Physics and Astronomy, University of California, Irvine, CA 92697, USA

^d Department of Chemical and Biomolecular Engineering, University of California, Irvine, CA 92697, USA

^{*}Correspondence to stacy.copp@uci.edu

have increased Stokes shifts and significantly suppressed visible CD transitions. Nanocluster electron count also significantly influences electronic structure and optical properties, with 6-electron and 8-electron Ag_N-DNAs exhibiting distinct absorbance and CD spectral features. This study shows that the optical and chiroptical properties of NIR-emissive Ag_N-DNAs are highly sensitive to nanocluster composition and illustrates the diversity of structure-property relationships for NIR-emissive Ag_N-DNAs, which could be harnessed to precisely tune these emitters for bioimaging applications.

Introduction.

DNA-stabilized silver nanoclusters¹ (Ag_N-DNAs) are emerging as promising emitters for applications in bioimaging and sensing.^{2,3} Ag_N-DNAs are known to consist of 10 to 30 Ag atoms protected by one or two single-stranded DNA oligomers, whose sequence selects the size, shape, and photophysical properties of the encapsulated silver nanocluster.⁴ Researchers have used this sequence-to-structure correlation to synthesize a diverse set of Ag_N-DNAs with atomically defined sizes and visible to near-infrared (NIR) emission wavelengths.⁴ NIR-emissive Ag_N-DNAs have recently gained particular attention for their high fluorescence quantum yields,⁵ large Stokes shifts,⁶ and unique photophysical properties for novel bioimaging modalities.^{7–10} High-throughput studies and machine learning-guided discovery have dramatically expanded the number of known NIR-emissive Ag_N-DNAs to hundreds of species.^{11,12} However, the fundamental structure-property relationships of this rapidly growing class of NIR emitters are poorly understood.

Detailed studies of compositionally pure Ag_N-DNAs over the last decade have particularly improved understanding of the compositions of Ag_N-DNAs with visible fluorescence wavelengths. Atomically precise Ag_N-DNA species can be isolated by high-performance liquid chromatography

(HPLC) and sized by high-resolution electrospray ionization mass spectrometry (ESI-MS) to determine the total number of silver atoms N, the number of DNA strands n_s , and the nanocluster charge Q_c of the Ag_N-DNA.^{4,13–16} With combined knowledge of N and Q_c , one can determine the nanocluster's effective valence electron count, $N_0 = N - Q_c$, which strongly influences nanocluster electronic structure¹⁷ and cannot be provided by crystallography alone. ESI-MS has shown that emissive Ag_N-DNAs are partially reduced, *i.e.* $N_0 < N$, and the dominant Ag_N-DNA excitation peak scales strongly with N_0 . The correlations of N_0 with excitation and emission energies are well-understood for visibly emissive Ag_N-DNAs: green-emissive Ag_N-DNAs have $N_0 = 4$ electrons, and red-emissive Ag_N-DNAs have $N_0 = 6$ electrons.^{16,18–20}

Far less is known about the compositions of NIR-emissive Agn-DNAs with peak emission wavelength $\lambda_{\rm p} > 700\,$ nm. Only a few NIR-emissive Agn-DNAs have molecular formulas determined by ESI-MS: four species with $\lambda_{\rm p} = 775\,$ to 1,000 nm and $N_0 = 10\,$ to 12 effective valence electrons; 11,16,20 two $N_0 = 8\,$ Agn-DNAs that show evidence for spherical geometries, like other 8-electron superatoms; 21 and the recently reported variants of a $N_0 = 6\,$ Ag16-DNA with $\lambda_{\rm p} = 735\,$ nm, an unusually large Stokes shift, two chlorido ligands, 22 and solved crystal structures. 23 Due to the varying affinities of adenine, cytosine, guanine, and thymine for silver cations, 24,25 the combinatorically large space of DNA oligomers may produce a wide array of Agn structures. Moreover, the significant diversities of Stokes shifts, quantum yields, excited state lifetimes, and dark state behaviors of Agn-DNAs in the NIR spectral range 6-9,20,21,26,27 further suggest that much about Agn-DNAs has yet to be understood.

To develop an understanding of the structure-property relationships of NIR Ag_N-DNA emitters, we investigate a large set of 19 different Ag_N-DNA species at the far red/NIR spectral border, with peak emission $\lambda_p = 640$ nm -820 nm. Several of these NIR Ag_N-DNAs have

previously attracted attention for their notable optical properties. 5,6,21–23 12 of the 19 Agn-DNAs in this study do not have molecular formulas assigned by ESI-MS, and only two have previously reported electronic circular dichroism (CD) spectra. We combine HPLC, high-resolution ESI-MS, and CD spectroscopy to correlate Agn core size, electron count, and ligand composition (*i.e.* the numbers of DNA ligands as well as chloride ligands) to optical properties. CD spectroscopy is especially sensitive to DNA molecular conformation and to the structural features of chiral metal nanoclusters, 28 and CD provides an important bridge with theory. 29 Agn-DNAs are known to exhibit UV and visible CD signatures, 19,30–33 but no large-scale study has correlated Agn-DNA CD signatures with their compositional or optical properties before. Moreover, the CD spectrum of the Ag16-DNA of known crystal structure was just recently calculated, 34 but the experimental CD spectrum of this emitter has not been reported prior to now.

This study shows that unlike the simpler N_θ -to-color correlation for green- and redemissive AgN-DNAs, NIR-emissive AgN-DNAs exhibit fluorescence spectra that depend on both valence electron count, N_θ , and ligand composition. Distinct UV and visible CD signatures are correlated with both the N_θ and the ligand content of AgN-DNAs, and ligand composition has a particular impact on the Stokes shifts of N_θ = 6 AgN-DNAs. Our measured CD spectrum for the chlorido-stabilized Ag₁₆-DNA also agrees well with very recent theoretical calculations.³⁴ This study illustrates the diversity of AgN-DNAs at the far red/NIR spectral border and shows that ligand chemistry can be used to precisely tune photophysical and chiroptical properties of these nanocluster emitters. Moreover, the compositional and spectral information provided here for a large set of 19 AgN-DNAs provide a rich data set to enable theoretical modeling of AgN-DNA electronic structure and inspire future X-ray crystallographic studies.

Results and Discussion.

We selected 19 Ag_N-DNAs with $\lambda_p = 640$ to 820 nm from a library of 10-base DNA oligomers previously designed using machine-learning methods. ^{12,35–37} Emitters were chosen for their λ_p values in the far-red to NIR spectral region and because they can be isolated by HPLC to obtain a compositionally pure species, which is an essential step that ensures only the emissive Ag_N-DNA species is probed by ESI-MS and CD spectroscopy. In addition to 15 NIR-emissive Ag_N-DNAs ($\lambda_p > 700$ nm), we also include four far-red emissive Ag_N-DNAs ($\lambda_p < 700$ nm) in order to compare to past studies on Ag_N-DNAs in the visible spectral window. ^{16,20} We consider only 10-base DNA oligomer length here because (1) these are by far the best-studied class of Ag_N-DNAs, with nearly 4,000 DNA sequences sampled to date, ^{5,6,11,12,16,20,35–38} and (2) by focusing on a single oligomer length, we separate the effects of DNA ligand length from DNA ligand conformation on Ag_N-DNA structural and optical properties.

Several NIR Ag_N-DNAs in this study were previously studied in detail. This includes emitters with molecular formulas determined by ESI-MS: a well-studied $\lambda_p = 735$ nm emissive (DNA)₂[Ag₁₆Cl₂]⁸⁺ and its variants with known structures^{23,39,40} and $N_0 = 6$;²² and two 8-electron species, (DNA)₂[Ag₁₆]⁸⁺ and (DNA)₂[Ag₁₇]⁹⁺.²⁶ Two other well-studied Ag_N-DNAs investigated here have unknown molecular formulas: a $\lambda_p = 721$ nm emitter with 73% quantum yield⁵ and a $\lambda_p = 811$ nm emitter with dual ns-lived and μ s-lived emission.²⁶ ESI-MS analysis of these latter two species may provide new insights into the origins of their favorable optical properties. About half of the 19 Ag_N-DNAs have never been studied in detail before.

Mass spectral analysis. Ag_N-DNAs were synthesized and then purified by ion-paired reverse-phase HPLC (chromatograms in **Figures S1 – S11**; details in Experimental Methods and Supporting Information **Table S1**). Following purification, we collected absorbance, emission, and

CD spectra for all Ag_N-DNAs. Composition was determined by negative ion mode ESI-MS, which is well-suited for characterizing noncovalent nucleic acid complexes. 41 Experimental mass spectra were fitted to determine each Ag_N-DNA's total silver content, N, valence electron count, N_0 , and the number of protecting DNA ligands, n_s , using previously established methods^{4,15,16,31} (see Supporting Information). Because ESI can remove Ag⁺ from or fragment Ag_N-DNA species, here we choose to assign Ag_N-DNA molecular formula to the largest mass product clearly resolved at multiple charge states, as in prior studies. 16,21 For 14 of the species, the largest mass product is also the most abundant product. For I.1, I.3, II.2, III.5, and IV.4, the largest mass product is less abundant than the second-largest mass product, which has one fewer Ag⁺. Past ESI-MS has shown that III.5 exhibits a largest mass product corresponding to N = 17 Ag atoms, ²² but crystallographic studies enable unambiguous assignment of the total silver content as N = 16 in that case. 40 Without available crystal structures, it is not possible to discriminate between silvers that are part of the Ag_N nanocluster core and Ag⁺ that are more weakly bound adducts, and thus choose to we assign N based on the largest clearly resolved mass spectral product at multiple charge states. We emphasize that isotopic distribution fits to each peak at multiple charge states show that total electron count, N_0 , for the largest and second-largest mass products are the same for **I.1**, **I.3**, **II.2**, III.5, and IV.4 (Table S3, Figures S12, S14, S18, and S21). Thus, it is possible that these Agn-DNAs have Ag+ that are more easily removed by ESI-MS than in other species. X-ray crystallography could be used to unambiguously assign total silver content, which is beyond the scope of this study.

Table 1 presents the molecular formulas of all 19 HPLC-purified Ag_N-DNAs, along with their peak absorbance wavelength(s) and emission wavelength λ_p . Mass spectral analyses to determine molecular formulas are provided in **Tables S2** and **S3**. To facilitate comparison in this

study, we group Ag_N-DNAs by ligand composition and N_{θ} . ESI-MS shows that the 6-electron Ag_N-DNAs ($N_{\theta} = 6$) possess three different types of ligand compositions: $n_s = 2$ DNA oligomers per nanocluster (*Group II*, example in **Figure 1a**), $n_s = 3$ DNA oligomers per nanocluster (*Group III*, example in **Figure 1b**), or $n_s = 2$ DNA oligomers and additional chlorido ligand(s) per nanocluster (*Group III*, example in **Figure 1c**). All four 8-electron Ag_N-DNAs ($N_{\theta} = 8$) are stabilized by $n_s = 2$ DNA oligomers (*Group IV*, example in **Figure 1d**). One mass spectrum for an Ag_N-DNA from each Group in **Table 1** is shown in **Figure 1**, and all other mass spectra are provided in **Figures S12 – S21**.

We find that all three of the far-red emissive AgN-DNAs in **Table 1** ($\lambda_p < 700$ nm) are 6-electron clusters with $n_s = 2$ DNA ligands (*Group I*) or with $n_s = 2$ DNA ligands and an additional chlorido ligand (*Group III*). 11 of the NIR emissive AgN-DNAs ($\lambda_p > 700$ nm) are 6-electron clusters (*Group II*, *Group III*), or *Group III*), while four are 8-electron clusters (*Group IV*). Notably, there is a significant overlap in λ_p values for $N_\theta = 6$ and $N_\theta = 8$ AgN-DNAs. This is unlike the distinct valence electron counts of green-emissive AgN-DNAs ($N_\theta = 4$) and red-emissive AgN-DNAs ($N_\theta = 6$), which had led to the notion of "magic colors" in this spectral range. Unlike the green-to-red spectral region, we find that peak emission wavelength in the far-red to NIR spectral region is not a sole indicator of AgN-DNA valence electron count, as we observe $N_\theta = 6$ AgN-DNAs at peak wavelengths up to $\lambda_p = 811$ nm and $N_\theta = 8$ AgN-DNAs at peak wavelengths as low as $\lambda_p = 720$ nm.

Table 1. Ag_N-DNA species grouped by valence electron content and ligand composition. N denotes the total number of silver atoms, N_0 denotes the valence electron counts, n_s is the number of DNA oligomers, Q_c is the nanocluster charge, and λ_p denotes the peak emission wavelength of the Ag_N-DNA. Within each group, emitters are ordered by λ_p .

Ag _N -DNA	DNA Sequence (5' to 3')	N	N_0	ns	Q _c	Abs / nm	$\lambda_{\rm p}$ / nm
Group I: Ag_N - $DNAs$ containing $N_0 = 6$ and $n_s = 2$							
<i>I</i> .1	GTCCGGGCCA	16	6	2	+10	530	639
<i>I</i> .2	ACCAATGACC	15	6	2	+9	545	650
<i>I</i> .3	CCAGCCCGGA	15	6	2	+9	560	660
<i>I</i> .4	GTAGTCCCTA	16	6	2	+10	560	720
<i>I</i> .5	ATCCCCTGTC	17	6	2	+11	582	727
<i>I</i> .6	AGTCACGACA ²⁶	16	6	2	+10	640	811
Group II: Ag_N -DNAs containing $N_0 = 6$ and $n_s = 3$							
<i>II</i> .1	CCCGGCCGAA	18	6	3	+12	630	703
II.2	CCCGGAGAAG ⁵	21	6	3	+15	640	721
II.3	CCTGGGGAAA	16	6	3	+10	651	726
Group III: Ag_N -DNAs containing $N_0 = 6$ with additional chlorido ligands							
III.1	AACCCCACGT ²²	15	6	2	+8	496	638
III.2	CACCTAGCGA ^{22,23}	16	6	2	+8	525	735
III.3	CACC <u>A</u> AGCGA ⁴⁰	16	6	2	+8	523	734
III.4	CACC <u>C</u> AGCGA ⁴⁰	16	6	2	+8	521	734
III.5	CACC <u>G</u> AGCGA ⁴⁰	16	6	2	+8	521	739
III.6	CACCTAGCG_ ³⁹	16	6	2	+8	522	754
<i>Group IV</i> : Ag_N - $DNAs$ containing $N_0 = 8$ and $n_s = 2$							
IV.1	GCGCAAGATG	19	8	2	+11	480, 615	720
IV.2	GACGACGGAT ²¹	17	8	2	+9	350, 410, 465	760
IV.3	ATCTCCACAG ²¹	16	8	2	+8	352, 452	800
<i>IV</i> .4	AGGCGATCAT	20	8	2	+12	355, 436, 500	820

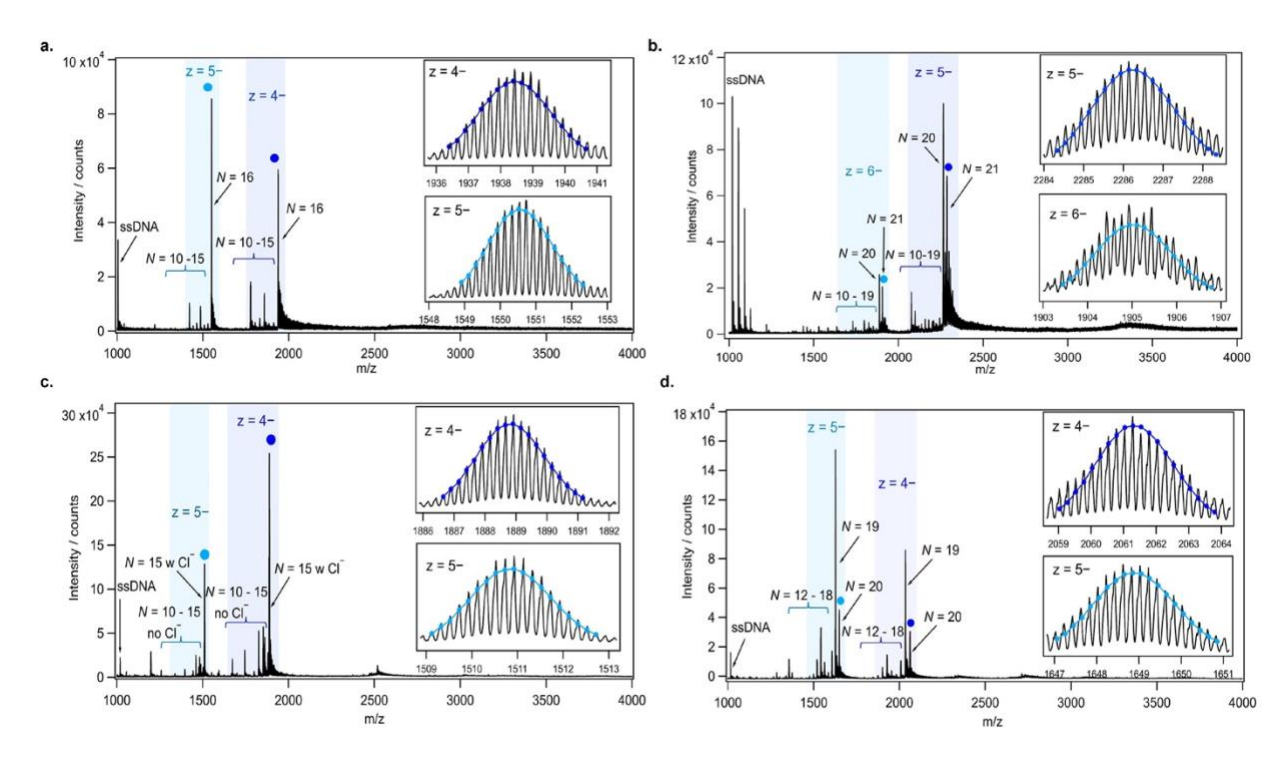


Figure 1. Mass spectra of **a. I.6**, **b. II.2**, **c. III.1**, and **d. IV.4**. Experimental data in black and peaks with different charge states of the Ag_N-DNA and different total numbers of silvers (*N*), and ssDNA are labelled. Insets show the experimental data fitted with isotopic distributions at different charge states (fitted peaks are labelled with respective colored circles).

Table 1 contains the molecular formulas of several notable and previously investigated Ag_N-DNAs whose compositions we determine here for the first time. We find that *I.*7, a $\lambda_p = 811$ nm emitter notable for exhibiting dual ns-lived and μ s-lived emission, 26 has molecular formula (DNA)₂[Ag₁₆]¹⁰⁺ (**Figure 2a**). The two dominant mass spectral peaks of *I.*7 at 1938.5 and 1550.5 m/z are well-fitted by calculated isotopic distributions for (DNA)₂[Ag₁₆]¹⁰⁺ at charge states of z = 4- and z = 5- (**Figure 2a** and **Table S2**), confirming that this species has a nanocluster charge of $Q_c = +10$ and an effective valence electron count of $N_0 = 16 - 10 = 6$. Mass spectra and isotopic distribution fits for other *Group I* Ag_N-DNAs are provided in **Figures S12 -S16** and **Table S2**, **S3**.

We also identify the first known Ag_N-DNAs stabilized by three copies of the DNA template oligomer ($n_s = 3$). This includes **II.2**, a previously reported $\lambda_p = 721$ nm NIR Ag_N-DNA that

exhibits an "unusually high" 73% quantum yield.⁵ Mass spectral analysis shows that II.2 has molecular formula (DNA)₃[Ag₂₁]¹⁵⁺, with $N_0 = 21 - 15 = 6$ valence electrons and $n_s = 3$ copies of the DNA template (**Figure 2b**). Notably, this finding validates the prior observation by Neacşu, *et al.* that the hydrodynamic volume of II.2, as measured by time-resolved anisotropy, is about twice as large as the volume of another NIR species with $n_s = 2$ DNA strands.⁵ We also identify two NIR-emitting $n_s = 3$ Ag_N-DNAs that have never been reported before: II.1, with $\lambda_p = 703$ nm and molecular formula (DNA)₃[Ag₁₈]¹²⁺, and II.3, with $\lambda_p = 726$ nm and molecular formula (DNA)₃[Ag₁₆]¹⁰⁺ (**Figure S17, S19**).

All three *Group II* n_s = 3 Ag_N-DNAs are significantly more prone to fragmentation during ESI-MS than n_s = 2 Ag_N-DNAs. (ESI-induced fragmentation is commonly observed for noncovalent DNA complexes,⁴¹ including Ag_N-DNAs.^{11,16,21,31–33,42}) For example, **Figure 2b** shows multiple mass spectral peaks corresponding to nanocluster products with N < 21 total silver atoms for *II.*2, in addition to the largest well-resolved mass spectral peak and its associated Na⁺ and NH₄⁺ adducts. *II.*1 and *II.*3 exhibit similar degrees of fragmentation (**Figures S17**, **S19**). We hypothesize that the greater propensity for ESI-induced fragmentation of *Group II* n_s = 3 Ag_N-DNAs as compared to *Group I* n_s = 2 Ag_N-DNAs is due to their greater hydrodynamic volume and generally larger values of total silver content N and cluster charge, Q_e , which could increase ESI-induced loss of more loosely bound Ag⁺ and DNA ligands from the Ag_N-DNAs. Moreover, Neacşu, *et al.*, previously observed that *II.*2 has limited thermal stability and therefore hypothesized that its high quantum yield results from a Ag_N core that is weakly bound to its DNA ligands, limiting solvent and/or DNA ligand-mediated nonradiative decay.⁵ Such a weaker Ag_N-ligand interaction is consistent with a greater degree of fragmentation by ESI for n_s = 3 Ag_N-DNAs.

Group III includes several recently reported Ag_N-DNAs with additional adventitious chlorido ligands and $N_0 = 6$ electrons. These chlorido-stabilized Ag_N-DNAs include III.2 through III.6, which are variants of a well-studied $\lambda_p = 735$ nm (DNA)₂[Ag₁₆Cl₂]⁸⁺ with known crystal structure, and III.1, a $\lambda_p = 638$ nm (DNA)₂[Ag₁₅Cl]⁸⁺ with one chlorido ligand²² (Figure 1c). We refer to the additional ligands as "chlorido" in accordance with IUPAC nomenclature.⁴³

Finally, *Group IV* includes two $N_0 = 8$ Ag_N-DNAs reported here for the first time, *IV.*1 and *IV.*4, and two previously reported $N_0 = 8$ Ag_N-DNAs²¹ (*IV.*2 and *IV.*3). Figure 2c shows the mass spectrum and isotopic fits for *IV.*4. Mass spectra and fit analysis for all $N_0 = 8$ Ag_N-DNAs are provided in **Table S3** and **Figure 1d**, **S20** -**S21**. We discuss later that compared to $N_0 = 6$ Ag_N-DNAs, *Group IV* Ag_N-DNAs exhibit highly complex absorbance spectra, without a single distinct peak in the visible spectral region. Thus, **Table 1** lists the wavelengths of the two to three well-defined near-UV to visible absorbance peaks for these emitters.

Relationship of molecular formula with Stokes shift. We next analyze the spectral properties and compositions in **Table 1** to determine whether general correlations exist between Ag_N-DNA composition and optical properties. Because three of the four $N_0 = 8$ Ag_N-DNAs do not have a single distinct longest wavelength absorbance transition, it is not appropriate to assign a single peak absorbance wavelength for these emitters, and we discuss these separately later. Here, we focus the discussion on $N_0 = 6$ Ag_N-DNAs. **Figure S22** shows no general correlation between peak emission and either N or Q_c for $N_0 = 6$ Ag_N-DNAs and weak correlation between peak absorbance and N or Q_c for $N_0 = 6$ Ag_N-DNAs; in the latter case, chlorido-stabilized Ag_N-DNAs (*Group III*) have generally lower peak absorbance wavelength than *Group I* and *II* Ag_N-DNAs without chlorido ligands, and $n_s = 3$ *Group II* Ag_N-DNAs have generally higher peak absorbance wavelength than $n_s = 2$ *Group I* Ag_N-DNAs. As discussed previously, ESI-induced removal of

silvers from less stable Ag_N-DNAs means that N and Q_c as measured by ESI-MS may not always represent the solution-phase total silver content N of an Ag_N-DNA. X-ray crystallography is needed to confirm N, and ESI-MS is needed to determine N_0 , which can be unambiguously determined by fitting the isotopic distribution of each peak in the mass spectrum. Crystallographic studies of more Ag_N-DNA species may improve correlations of peak absorbance/emission and either N or Q_c .

When λ_p is plotted against the longest wavelength absorbance peak, we observe that the emitters are roughly grouped by ligand composition, specifically, by the value of n_s and the presence or absence of additional chlorido ligands (**Figure 2a**). This suggests differences in Stokes shift magnitude among *Group II*, *Group III*, and *Group III* emitters. **Figure 2b** confirms these differences, displaying Stokes shift in units of energy (eV) as a function of peak absorbance energy. *Group II* Agn-DNAs with $n_s = 3$ DNA oligomer ligands possess substantially smaller

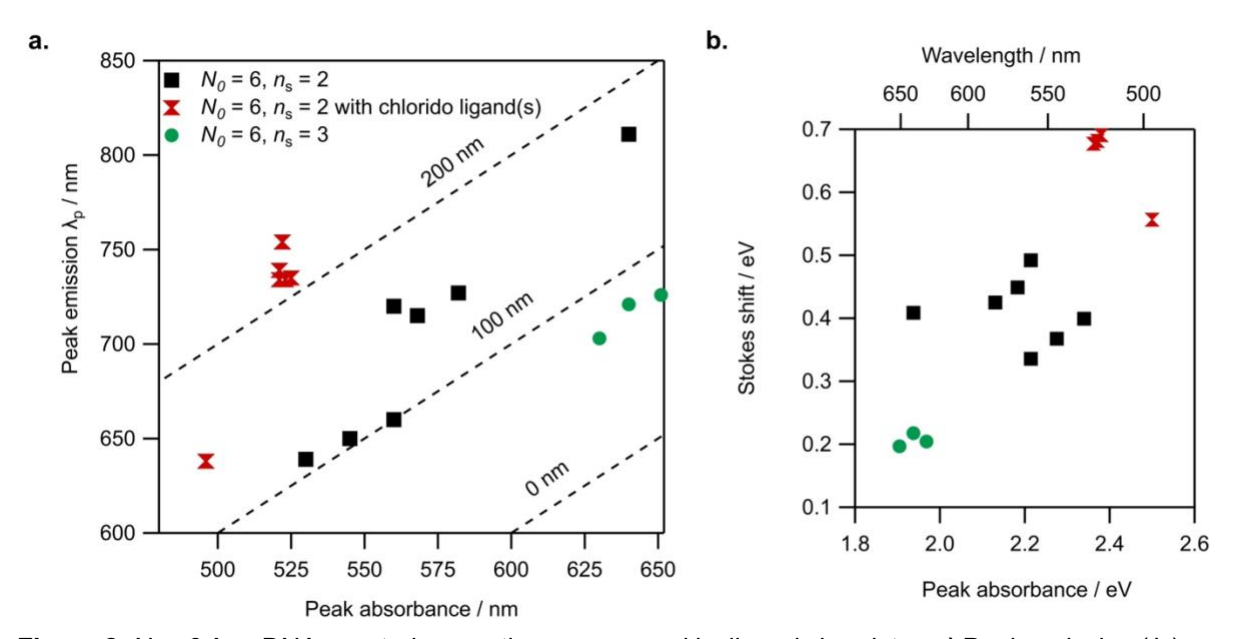


Figure 2. N_0 = 6 Ag_N-DNA spectral properties are grouped by ligand chemistry. **a)** Peak emission (λ_p) *versus* peak absorbance wavelength for *Group II* (black squares), *Group II* (green circles), and *Group III* (red double triangles). Dotted lines represent absorbance and emission values corresponding to 0 nm, 100 nm, and 200 nm Stokes shift. **b)** Stokes shift *versus* peak absorbance (units of energy) for N_0 = 6 Ag_N-DNAs. Note: for *Group III* Ag_N-DNAs, *III.*2 through *III.*6 are essentially the same emitter^{39,40} and thus have nearly equivalent absorbance and emission values.

Stokes shifts than *Group I* Ag_N-DNAs, and *Group III* Ag_N-DNAs exhibit significantly larger Stokes shifts than other $N_0 = 6$ Ag_N-DNAs. Given the trends in **Figure S22c,d** these experimental findings support that ligand chemistry has significant effects on the ground state energy levels and the excited-state energy loss (Stokes shift) of Ag_N-DNAs at the far-red/NIR spectral border. Recent theoretical analysis of the frontier orbitals of *III.6*, one of the (DNA)₂[Ag₁₆Cl₂]⁸⁺ with known crystal structure, found that most of the frontier orbitals have significant weight on the inorganic Ag₁₆Cl₂ core.³⁴ Thus, it is likely that chlorido ligands in this inorganic core will have an effect on ground state and excited state processes of Ag_N-DNAs.

Circular dichroism signatures. We next investigate how the chiroptical signatures of N_0 = 6 Ag_N-DNAs correlate with ligand composition. CD spectroscopy is a powerful tool for characterizing Ag_N-DNAs because of its sensitivity to DNA conformation^{44,45} and its ability to interrogate the origins of electronic transitions in monolayer-protected metal nanoclusters, in combination with theoretical calculations.²⁸ CD signatures in the 200 to 320 nm UV spectral region are assumed to primarily originate from the nucleobases and their interaction with the nanocluster core. Because DNA itself exhibits no chiroptical activity above ca. 320 nm, higher-wavelength CD signatures are assumed to arise due to electronic transitions in the nanocluster. Thus, CD studies of Ag_N-DNAs could provide information about both DNA ligand conformation and Ag_N core geometry and electronic structure.

All past CD studies of purified Ag_N-DNAs have reported a distinct monosignate CD transition aligned with the longest wavelength visible or NIR absorbance peak. $^{19,30-33}$ Four Ag_N-DNAs with $N_0 = 4$, 6, and 12 were found to exhibit positive Cotton effect for the CD transition aligned with the longest wavelength absorbance peak, as well as six similar UV CD transitions that suggest similar DNA ligand conformations despite widely differing DNA oligomer lengths

and Ag_N-DNA compositions. Quantum chemical calculations qualitatively replicated the seven major CD transitions, 30,46 although X-ray crystallography has since shown that thread-like Ag_N are unrealistic models for Ag_N-DNAs. 23,47 Density functional theory calculations of a $N_0 = 4$ Ag_N-DNA predicted positive monosignate CD transition aligned with the longest-wavelength absorbance peak. In contrast, Petty and coauthors more commonly report negative Cotton effect aligned with the longest-wavelength absorbance peaks of green-emissive Ag_N-DNAs. $^{19,31-33}$

Varying chirality in 6-electron Agn-DNAs. We find that all $N_0 = 6$ Agn-DNAs stabilized by $n_s = 2$ or 3 DNA strands (*Groups I* and *II*, respectively) exhibit well-defined monosignate CD transitions aligned with the longest-wavelength absorbance peak (**Figures 3, 4**). These transitions are negative Cotton peaks for all *Group I* and *II* emitters except *I.*2 ($\lambda_p = 650$ nm), which exhibits a strong positive Cotton effect at the longest wavelength absorbance peak (**Figure 3b**). The significant prevalence of these negative CD transitions exhibited by *Group I* and *II* $N_0 = 6$ Agn-DNAs contrasts with reports by Swasey, *et al.*, of only positive Cotton effect at visible wavelengths for two $N_0 = 6$ Agn-DNAs stabilized by $n_s = 1$ DNA ligands of 28 and 34 nucleobases. ³⁶ Our results support that short DNA oligomers can stabilize $N_0 = 6$ Agn-DNAs with either chiral handedness, even for Agn of identical size (*I.*2 and *I.*3 both contain N = 15, $N_0 = 6$, and $n_s = 2$). This illustrates the diversity of nanocluster chiralities that can be achieved with DNA oligomer ligands.

UV CD signatures of Agn-DNAs. Figure 3 shows that Group I Agn-DNAs exhibit a greater diversity of UV CD features than the four Agn-DNAs reported by Swasey, et al. This may suggest a variety of DNA conformations around the nanocluster core for Group I Agn-DNAs. We note that II.2, the only Group I Agn-DNA with a positive long-wavelength CD peak, exhibits solely negative CD in the UV region, unlike the other five Group I Agn-DNAs. More emitters

should be investigated to determine if UV CD features correlate with the sign of the dominant visible CD feature for Ag_N-DNAs.

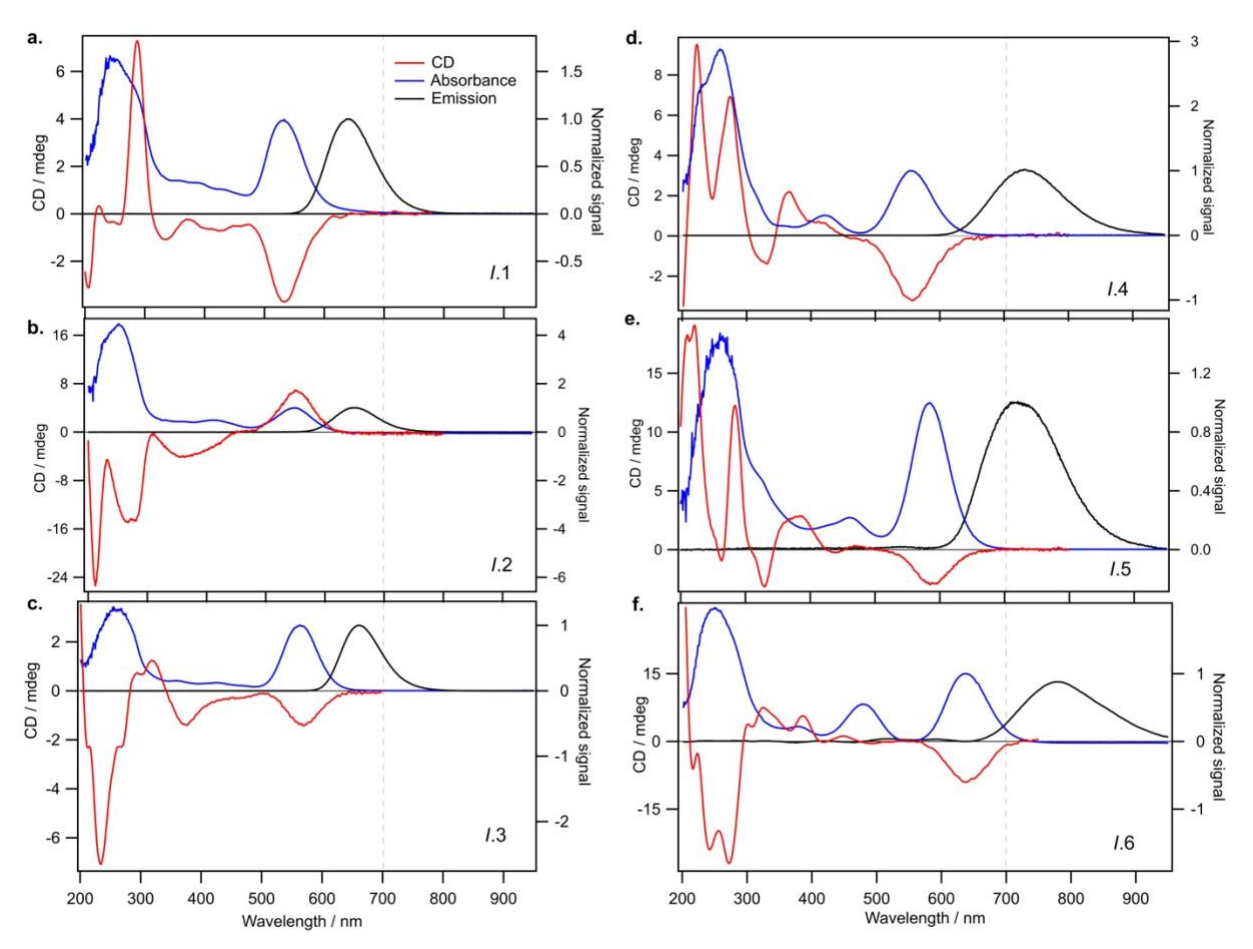


Figure 3. CD (red), absorbance (blue), and emission (black) of *Group I* Ag_N-DNAs containing N_0 = 6 and stabilized by n_s = 2 DNA oligomers. Fluorescence emission spectra are excited at 260 nm, which universally excites all emissive Ag_N-DNA species. The vertical dashed line at 700 nm indicates the far-red to NIR wavelength boundary.

Group II Ag_N-DNAs ($n_s = 3$ DNA strands) share markedly similar UV CD signatures, unlike the more diverse **Group** I Ag_N-DNAs. **Figure 4** shows that all **Group** II Ag_N-DNAs exhibit negative CD transitions aligned with the longest wavelength absorbance peak and that their UV CD spectra possess distinctly similar transitions, including a strong negative Cotton effect at ca. 216 nm, a positive Cotton effect at ca. 300 nm, and a negative Cotton effect around 340 – 375 nm

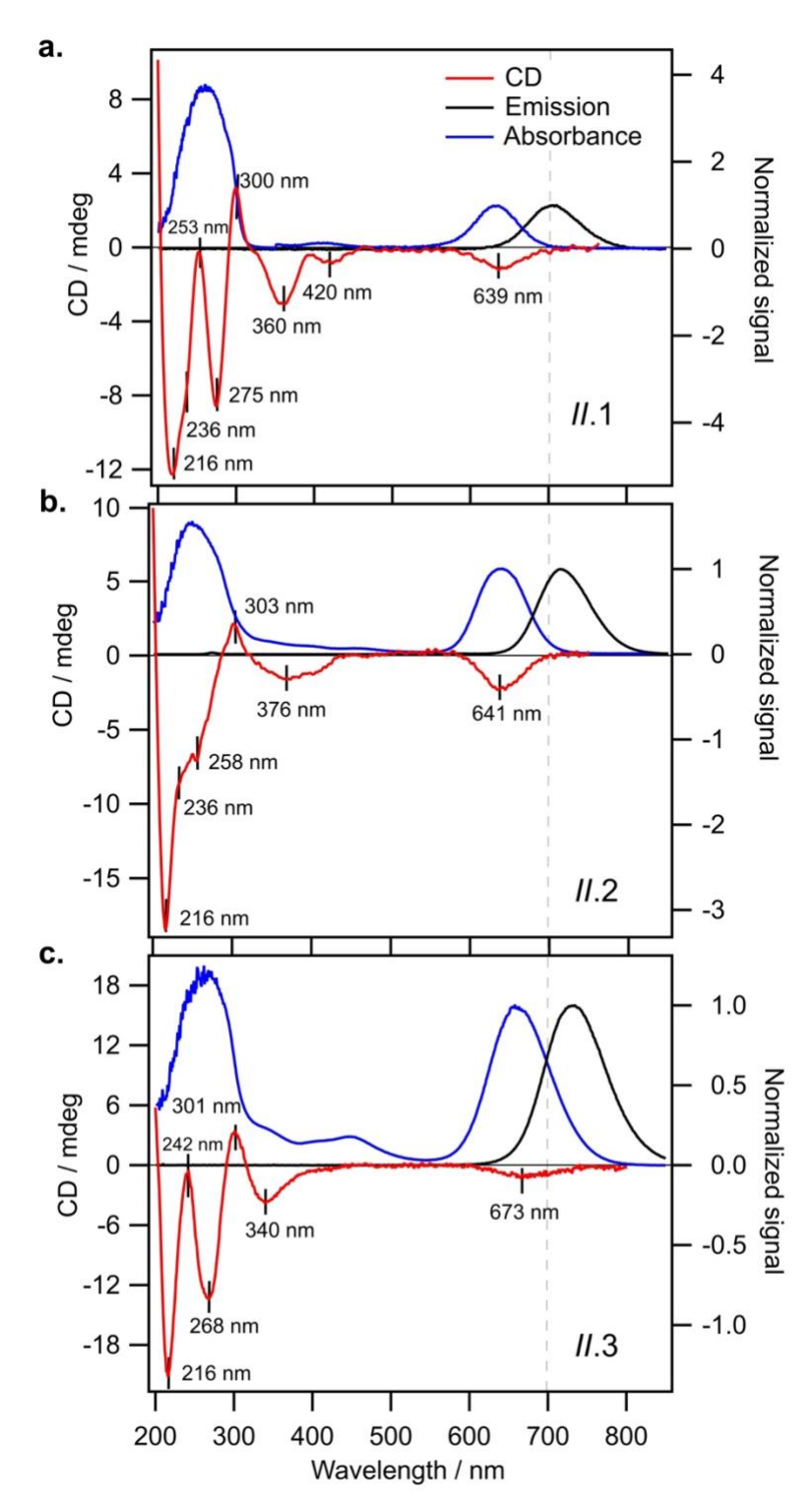


Figure 4. CD (red), absorbance (blue), and emission (black) spectra of *Group II* Ag_N-DNAs with n_s = 3 DNA strands and N_0 = 6 electrons. a) *II.*1, b) *II.*2, and c) *II.*3 exhibit similar UV CD signatures and a single dominant negative CD transition aligned with the peak visible absorbance wavelength. The vertical dashed line at 700 nm indicates the far-red to NIR wavelength boundary.

(**Figure 4**). This high degree of spectral similarity suggests shared conformations of the DNA oligomer ligands around the central Ag_N for all $n_s = 3$ Ag_N-DNAs. However, the significant differences between natural DNA secondary structures and the conformation of DNA ligands on the few Ag_N-DNAs with known crystal structures^{23,39,40,47} limit the use of well-established CD-to-structure correlations for natural DNA to interpret the structures of Ag_N-DNA ligands. Given that *II.2* is reported to exhibit unusually high 73% quantum yield,⁵ it is important to understand and learn how to design for the ligand conformation of $n_s = 3$ Ag_N-DNAs. We encourage experimental work to crystalize and solve the structures of $n_s = 3$ Ag_N-DNAs, together with theoretical studies to provide better understanding of the origins of their optical properties.

Effects of chlorido ligands on CD signatures. All Group III Agn-DNAs, which are stabilized by both DNA and chlorido ligands, exhibit highly diminished CD signals at visible wavelengths (Figure 5), in contrast with the well-defined CD signatures of Groups I, II, and IV Agn-DNAs (Figures 3, 4, 6). Figure 5c compares the CD spectra of five variants of the same (DNA)₂[Ag₁₆Cl₂]⁸⁺, all solved by X-ray crystallography^{23,39,40} (sequences in legend). We observe experimentally that (DNA)₂[Ag₁₆Cl₂]⁸⁺ variants either exhibit no CD signal or very weak positive CD signal at ca. 500 to 600 nm (Figure 5c). The slight differences in CD spectra of these variants likely result from slight differences in Ag₁₆ structure and ligand conformation as a result of single-base differences in the DNA templates.⁴⁰

Malola, *et al.*, recently used linear response time-dependent density functional theory to calculate ground state absorbance and CD spectra of the "A10" variant, *III.*6.³⁴ Their study represents the first such theoretical analysis for realistic Ag_N-DNA systems. The calculated ground state absorbance spectrum agreed well with the experimental absorbance spectrum (**Figure 5b**), matching the three dominant absorbance peaks in the 300 to 550 nm spectra region. They also

predicted the emitter's CD spectrum to exhibit weak, negative signal in the 500 to 600 nm spectral region and more intense UV CD features. The UV features and suppressed CD signal at visible wavelengths agree with our experimental findings in **Figure 5c**, and the suppressed visible CD signal is also in agreement with the weak nanocluster chirality of the X-ray crystal structure of *III.6*. There is, however, a slight discrepancy in the sign of this weak CD signal in **Figure 5c** as compared to predictions by Malola, *et al*. We hypothesize that this discrepancy may arise from solution-state dynamics of the nanocluster core that were not captured in the calculations. More detailed theoretical studies of nanocluster dynamics may shed light on this discrepancy. We note that the spectra we provide in **Figure 5c** would enable a detailed comparison of calculated CD spectra for all five variants of the (DNA)₂[Ag₁₆Cl₂]⁸⁺ emitter.

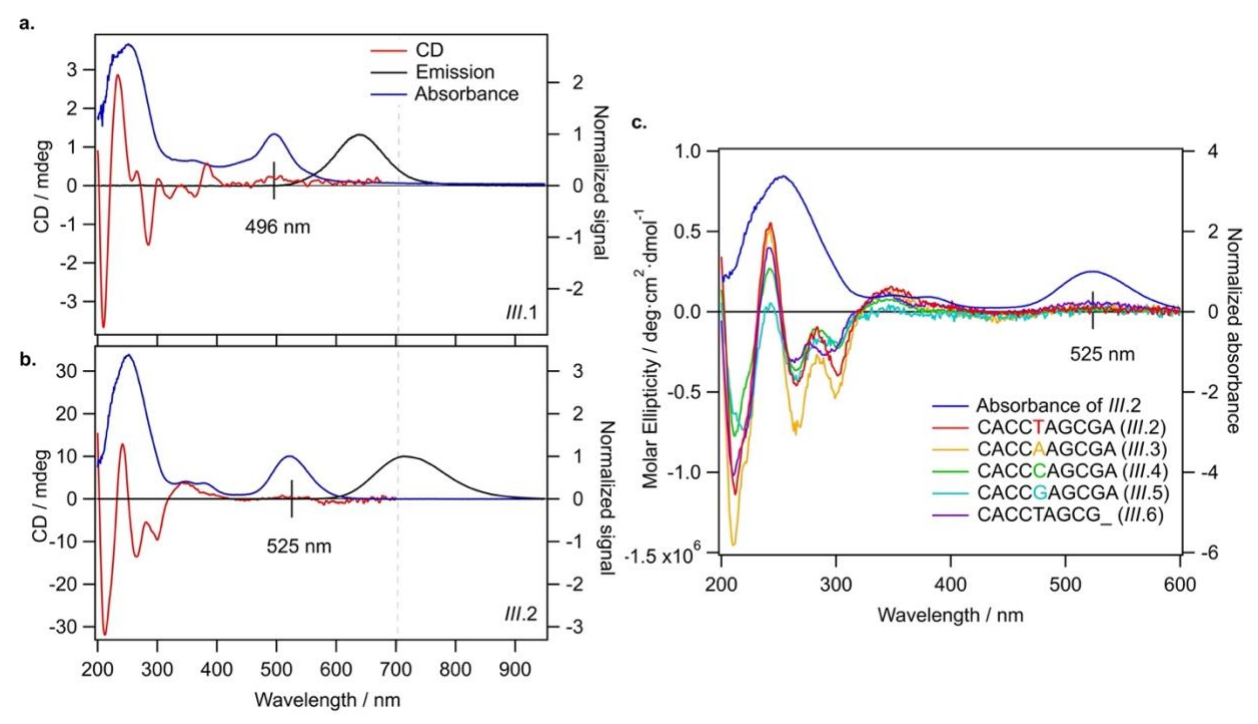


Figure 5. CD (red), absorbance (blue), and emission (black) spectra of *Group III* Ag_N-DNAs stabilized with additional chlorido ligands. **a)** *III.*1 and **b)** *III.*2 exhibit highly suppressed CD signatures at visible wavelengths (indicated at 496 nm and 525 nm for *III.*1 and *III.*2, respectively. The vertical dashed line at 700 nm indicates the far-red to NIR wavelength boundary. **c)** CD spectra of all variants of *III.*2, including *III.*3 through *III.*6, reported in units of molar ellipticity.

While further theoretical studies are needed to fully understand the origins of chiroptical activity of Ag_N-DNAs, the crystal structures of *III.2* through *III.6* do provide hints. These Ag₁₆ nanoclusters have two chlorido ligands bound to the long faces of the nanocluster with a highly symmetric coordination structure.^{22,23,39} It may be that chlorido ligands act to "straighten out" the Ag₁₆, reducing its structural chirality and thereby suppressing the CD spectral features that correspond to the lowest-energy excitations of the nanocluster rod,³⁴ which are much more intense in *Group I* and *III* Ag_N-DNAs. Crystallographic studies of Ag_N-DNAs without chlorido ligands are needed to test this hypothesis. Moreover, crystallographic studies of *III.1* are needed to determine the position of its single chlorido ligand and discern how this ligand affects nanocluster chirality and chiroptical activity.

Comparison of 6-electron and 8-electron Ag_N -DNAs. Lastly, we examine the optical and chiroptical properties of $Group\ IV$ Ag_N -DNAs (with $N_0 = 8$ valence electrons). This includes the two $N_0 = 8$ Ag_N -DNAs that we report for the first time, IV.1 and IV.4, and the previously reported IV.2 and IV.3.²¹ These emitters exhibit clearly distinct absorbance spectral features compared to all $N_0 = 6$ Ag_N -DNAs. The four $Group\ IV$ emitters exhibit multiple distinct absorbance peaks in the near-UV and visible spectral regions (Figure 6, blue curves), unlike the single dominant peak in the visible spectral region that is exhibited by $N_0 = 6$ Ag_N -DNAs. IV.1 is the only $N_0 = 8$ emitter with a well-defined high-wavelength absorbance peak, which we hypothesize is due to a slightly different nanocluster geometry than IV.2 through IV.4, which exhibit poorly defined low-intensity absorbance features above ca. 500 nm and significant UV-to-VIR down-conversion, as previously reported for IV.2 and IV.3.²¹

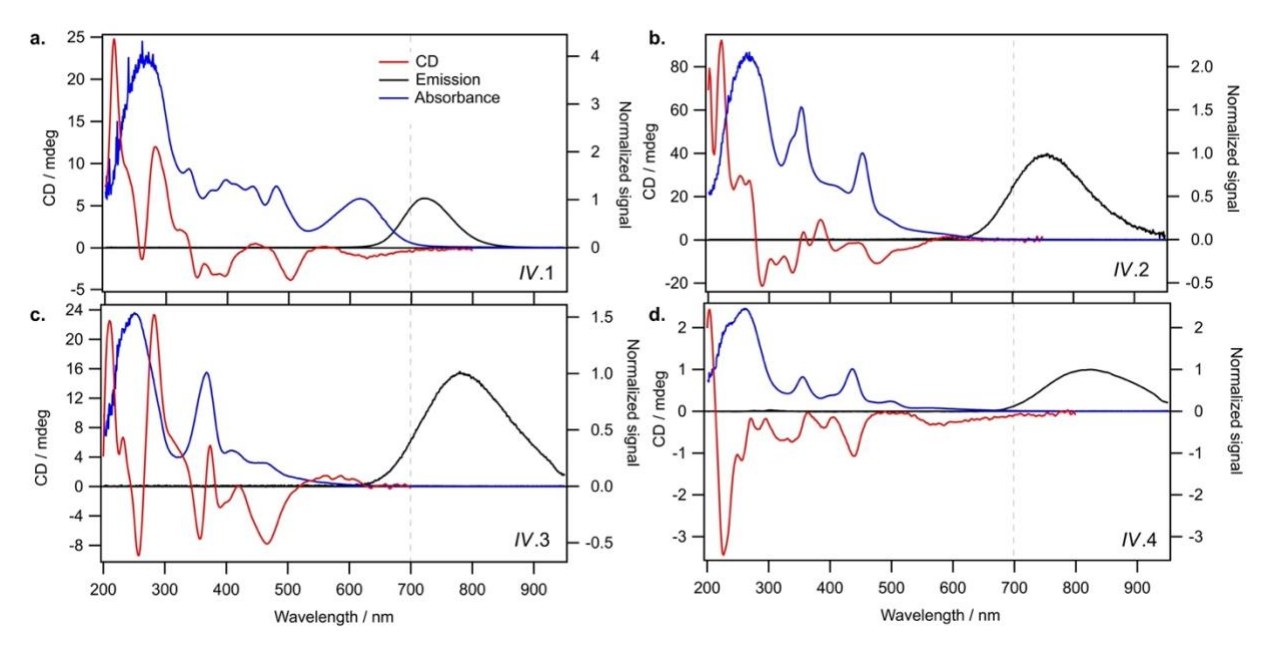


Figure 6 CD (red), absorbance (blue), and emission (black) spectra of *Group IV* Ag_N-DNAs containing N_0 = 8 and stabilized by two strands of DNA oligomers (n_s = 2). The vertical dashed line at 700 nm indicates the far-red to NIR wavelength boundary.

The spectral differences between *Groups I* and *IV* clearly illustrate the role of electron count, N_0 , on Ag_N-DNA optical properties. *Groups I* and *IV* have differing N_0 , despite both being stabilized by $n_s = 2$ 10-base oligonucleotide ligands per Ag_N. The complex absorbance spectra of *Group IV* Ag_N-DNAs (**Figure 6**) are in clear contrast with the simpler absorbance spectra of *Group I* Ag_N-DNAs, which exhibit a single dominant long wavelength absorbance peak and either less intense peaks or extremely subtle features at shorter near-UV to visible wavelengths (**Figure 3**). The CD spectra of *Group IV* Ag_N-DNAs ($N_0 = 8$) are also more complex than *Groups I*, *II*, *III* ($N_0 = 6$). This includes the newly reported CD spectra of *IV*.1 and *IV*.4 and the previously reported CD spectra of *IV*.2 and *IV*.3.²¹ The distinct differences between the chiroptical and optical properties of superatomic $N_0 = 8$ Ag_N-DNAs and $N_0 = 6$ Ag_N-DNAs indicate differences in nanocluster electronic structure and strongly suggest fundamental differences in nanocluster shape. $N_0 = 6$ Ag_N-DNAs are either known or expected to be rod-shaped. ^{15,16,18,23} $N_0 = 8$ Ag_N-DNAs are

hypothesized to possess pseudo-spherical shapes, similar to other ligand-protected 8-electron nanocluster superatoms.²¹ Thus, N_0 plays a clear role in determining the geometry and ground state electronic structure of Ag_N-DNAs, and differences in N_0 produce different classes of NIR Ag_N-DNA emitters.

Significant current research is focused on the fundamental mechanisms and synthetic control of the chiroptical properties of ligand-protected nanoclusters. ^{28,49–55} CD spectroscopy is highly sensitive to a nanocluster's core, its ligand-core interface, and its ligand shell. Chiroptical signatures of nanoclusters often have complex origins, arising from interactions among the metal cluster core, ligand-metal units, and/or surrounding ligand groups, ⁵⁰ and theoretical studies using structures from X-ray crystallography are often required to elucidate the origins of these CD spectral features. In some cases, chirality transfer from ligand to nanocluster results in strong chiroptical signatures. ⁵¹ Chirality transfer from metal nanoclusters to adsorbates has also been observed and is of importance for heterogeneous enantioselective catalysis. ⁴⁹ Thus, research into the origins of chiroptical properties of Ag_N-DNAs will not only advance the fundamental chemistry of nanocluster systems but also has important potential technological applications.

To our knowledge, this is the first detailed study of how the molecular formulas of far red to NIR-emissive Ag_N-DNAs dictate their structure and chiroptical properties. Our results show that multidentate DNA ligands are versatile templates for a diverse set of nanocluster structures, with optical properties influenced by *both* electron count N_0 and ligand composition. Variations in electron count and ligand composition produce at least four different classes of NIR-emissive Ag_N-DNAs with distinct optical properties, and it is possible that an even richer space of possible emitters has yet to be discovered.

While the major experimental challenges of growing single crystals of Agn-DNAs that are suitable for single crystal X-ray diffraction continues to limit progress in understanding their structure-property relationships, this study demonstrates that ESI-MS combined with UV/Vis and CD spectroscopy provides an alternate approach to advance understanding of the solution-phase structures of Agn-DNAs. Moreover, because ground state absorbance and CD spectra can be calculated using *ab initio* models, the large set of experimental absorbance, emission, and CD spectra of Agn-DNAs presented here will enable theoretical groups to model these emitters while awaiting more X-ray crystal structures to be solved. Importantly, our reports include electron counts for all 19 Agn-DNAs in this study, which are critical for accurate *ab initio* calculations of their electronic structure.

Conclusions. In summary, we have investigated the compositions and optical properties of 19 atomically precise Agn-DNA species emitting in the far-red to NIR spectral region, each stabilized by a different 10-base DNA oligomer. Molecular formulas determined by ESI-MS show that Agn-DNAs emitting in this spectral region can possess either 6 or 8 total valence electrons (N_0) and that unlike visibly emissive Agn-DNAs, emission wavelength in the far red/NIR spectral region is not a sole indicator of electron count. 6-electron Agn-DNAs have diverse ligand compositions, which appears to strongly influence Stokes shift. Agn-DNAs stabilized by $n_s = 3$ DNA ligands are identified here for the first time, and these exhibit longer wavelength absorbance peaks and shorter Stokes shifts (70 to 80 nm) than Agn-DNAs stabilized by $n_s = 2$ DNA ligands. Additional chlorido ligands are correlated with shorter wavelength absorbance peaks and larger Stokes shifts. UV CD signatures further suggest structural differences in DNA ligand conformation and/or nanocluster chirality amongst the three classes of 6-electron Agn-DNAs. In particular, Agn-DNAs protected

solely by DNA ligands have well-defined visible CD transitions, while chlorido-protected Agn-DNAs have significantly suppressed visible CD transitions, agreeing well with emerging theoretical studies and suggesting a lower degree of nanocluster chirality when chlorido ligands are present. Finally, major distinctions exist between both the optical and chiroptical signatures of 8-electron Agn-DNAs versus 6-electron Agn-DNAs, which likely result from significant structural differences in the Agn core geometries of 6-electron and 8-electron nanoclusters and the conformations adopted by their DNA ligands. This work may enable future computational studies to understand the origins of the chiroptical properties of Agn-DNAs. Future efforts to solve the X-ray crystal structures of these Agn-DNAs would significantly expedite the progress of such computational studies, and we hope that researchers will attempt to crystallize the emitters presented here.

Experimental Section

Synthesis and purification of AgN-DNAs. AgN-DNAs were synthesized by the addition of stoichiometric amounts of AgNO₃ (see SI) to an aqueous solution of DNA oligomer (Integrated DNA Technologies, standard desalting) in 10 mM ammonium acetate, followed by the partial reduction of the silver content using 0.5 molar ratio of a freshly prepared aqueous solution of NaBH₄. For emitter *IV*.4 only, an elevated storage temperature above 4 °C was used after chemical reduction to form the NIR-emissive species. ⁵⁶ To achieve high enough yields for CD spectroscopy, 5 to 15 mL of solution was typically prepared. The solution was kept at 4 °C (or stated otherwise) in dark until concentration by spin filtering and then purification using reverse-phase HPLC (See SI). Following HPLC, the solvent was exchanged into 10 mM ammonium acetate, pH 7.

Mass spectrometry. Electrospray ionization mass spectrometry (ESI-MS) was performed using a Waters Xevo G2-XS QTof. Samples were directly injected at 0.1 mL/min in negative ion mode with a 2 kV capillary voltage, 30 V cone voltage and no collision energy. Spectra were collected from 1000 to 4000 m/z with an integration time of 1 s. Source and desolvation temperatures were 80 and 150 °C, respectively. Gas flows were 45 L/h for the cone, and 450 L/h for the desolvation. Samples were injected with 50 mM NH₄OAc – MeOH (80:20) solution at pH 7. These solvent and ESI-MS settings were chosen to minimize product fragmentation from a range of tested conditions, inspired by prior work. ^{13,15,41} Determination of nanocluster size (total number of silvers N, ligand composition *i.e.*, the number of DNA strands n_s , and the presence of additional chlorido ligands) and the overall charge, Q_c (and hence determine the number of effective neutral silvers N_0) was performed by fitting the calculated isotopic distribution of the Ag_N-DNA to the experimental spectra (details in SI). Calculated isotopic distributions were obtained from MassLynx using the chemical formula and corrected for the overall positive charge (oxidation state, Q_c) of the nanocluster core.

Optical characterization. Steady-state absorbance and emission spectra were recorded using a thermoelectrically cooled, fiber-coupled spectrometer (Ocean Optics QE65000). Absorbance spectra were collected using a DH-Mini (Ocean Insight) deuterium & tungsten halogen UV-Vis-NIR light source. Fluorescence spectra were collected using a UV LED for universal UV excitation.⁵⁷ Circular dichroism measurements were performed on Chirascan V100 from Applied Photophysics. The concentration of samples was maintained such that the absorbance of the Ag_N-DNA ranged between 0.8 to 1.0. The CD spectra of Ag_N-DNA in 10 mM ammonium acetate were recorded from 200 to 800 nm in a quartz cuvette (Starna Cells) of 0.5 mm optical path length at 20 °C with a scanning rate of 1.0 nm interval per 1.0 s. The CD spectrum of each Ag_N-DNA is the

average of three scans with a manual baseline correction to remove contributions from 10 mM NH₄OAc.

Acknowledgements: This work was supported by NSF Biophotonics CBET-2025790 and AFOSR FA9550-21-1-0163 and AFOSR DURIP FA9550-22-1-0206. A.G.-R. acknowledges a Balsells Graduate Fellowship. M. R. acknowledges a UC Irvine Engineering Pathway to the PhD Fellowship. The authors thank Hannu Häkkinen and Ara Apkarian for helpful discussions.

Supporting Information: Materials and experimental methods; HPLC chromatograms; mass spectra and associated calculated mass distributions.

Conflicts of interest: There are no conflicts to declare.

References

- J. T. Petty, J. Zheng, N. V Hud and R. M. Dickson, *J. Am. Chem. Soc.*, 2004, **126**, 5207–12.
- 2 Y. Chen, M. L. Phipps, J. H. Werner, S. Chakraborty and J. S. Martinez, *Acc. Chem. Res.*, 2018, **51**, 2756–2763.
- R. Guha and S. M. Copp, in *Modern Avenues in Metal-Nucleic Acid Chemistry*, eds. J. Müller and B. Lippert, CRC Press, 25th edn., 2023, pp. 291–342.
- 4 A. Gonzàlez-Rosell, C. Cerretani, P. Mastracco, T. Vosch and S. M. Copp, *Nanoscale Adv.*, 2021, **3**, 1230–1260.
- 5 V. A. Neacşu, C. Cerretani, M. B. Liisberg, S. M. Swasey, E. G. Gwinn, S. M. Copp and T. Vosch, *Chem. Commun.*, 2020, **56**, 6384–6387.
- S. A. Bogh, M. R. Carro-Temboury, C. Cerretani, S. M. Swasey, S. M. Copp, E. G. Gwinn and T. Vosch, *Methods Appl. Fluoresc.*, 2018, **6**, 024004.
- 7 M. B. Liisberg, Z. S. Kardar, S. M. Copp, C. Cerretani and T. Vosch, *J. Phys. Chem. Lett.*, 2021, **12**, 1150–1154.
- 8 S. Krause, M. R. Carro-Temboury, C. Cerretani and T. Vosch, *Phys. Chem. Chem. Phys.*, 2018, **20**, 16316–16319.
- 9 S. Krause, M. R. Carro-Temboury, C. Cerretani and T. Vosch, *Chem. Commun.*, 2018, **54**, 4569–4572.
- 10 S. Krause, C. Cerretani and T. Vosch, *Chem. Sci.*, 2019, **10**, 5326–5331.
- 11 S. M. Swasey, S. M. Copp, H. C. Nicholson, A. Gorovits, P. Bogdanov and E. G. Gwinn, *Nanoscale*, 2018, **10**, 19701–19705.
- P. Mastracco, A. Gonzàlez-Rosell, J. Evans, P. Bogdanov and S. M. Copp, ACS Nano,

- 2022, **16**, 16322–16331.
- 13 D. Schultz and E. G. Gwinn, *Chem. Commun. (Camb).*, 2012, **48**, 5748–50.
- 14 K. Koszinowski and K. Ballweg, *Chem. A Eur. J.*, 2010, **16**, 3285–3290.
- D. Schultz, K. Gardner, S. S. R. Oemrawsingh, N. Markešević, K. Olsson, M. Debord, D. Bouwmeester and E. Gwinn, *Adv. Mater.*, 2013, **25**, 2797–803.
- S. M. Copp, D. Schultz, S. Swasey, J. Pavlovich, M. Debord, A. Chiu, K. Olsson and E. Gwinn, *J. Phys. Chem. Lett.*, 2014, **5**, 959–963.
- 17 H. Häkkinen, *Chem. Soc. Rev.*, 2008, **37**, 1847–59.
- 18 S. M. Copp, D. Schultz, S. M. Swasey, A. Faris and E. G. Gwinn, *Nano Lett.*, 2016, **16**, 3594–3599.
- J. T. Petty, M. Ganguly, I. J. Rankine, E. J. Baucum, M. J. Gillan, L. E. Eddy, J. C. Léon and J. Müller, *J. Phys. Chem. C*, 2018, **122**, 4670–4680.
- 20 S. M. Copp and A. Gonzàlez-Rosell, *Nanoscale*, 2021, **13**, 4602–4613.
- A. Gonzàlez-Rosell, R. Guha, C. Cerretani, V. Rück, M. B. Liisberg, B. B. Katz, T. Vosch and S. M. Copp, *J. Phys. Chem. Lett.*, 2022, **13**, 8305–8311.
- A. Gonzàlez-Rosell, S. Malola, R. Guha, N. R. Arevalos, M. F. Matus, M. E. Goulet, E. Haapaniemi, B. B. Katz, T. Vosch, J. Kondo, H. Häkkinen and S. M. Copp, *J. Am. Chem. Soc.*, 2023, **145**, 10721–10729.
- 23 C. Cerretani, H. Kanazawa, T. Vosch and J. Kondo, *Angew. Chem. Int. Ed.*, 2019, **58**, 17153–17157.
- S. M. Swasey, L. E. Leal, O. Lopez-Acevedo, J. Pavlovich and E. G. Gwinn, *Sci. Rep.*, 2015, **5**, 10163.
- 25 S. M. Swasey, F. Rosu, S. M. Copp, V. Gabelica and E. G. Gwinn, *J. Phys. Chem. Lett.*, 2018, **9**, 6605–6610.
- V. Rück, C. Cerretani, V. A. Neacşu, M. B. Liisberg and T. Vosch, *Phys. Chem. Chem. Phys.*, 2021, **23**, 13483–13489.
- 27 J. T. Petty, S. Carnahan, D. Kim and D. Lewis, *J. Chem. Phys.*, 2021, **154**, 244302.
- 28 S. Knoppe and T. Burgi, Acc. Chem. Res., 2014, 47, 1318–1326.
- 29 K. L. D. M. Weerawardene, H. Häkkinen and C. M. Aikens, *Annu. Rev. Phys. Chem.*, 2018, **69**, 205–229.
- 30 S. M. Swasey, N. Karimova, C. M. Aikens, D. E. Schultz, A. J. Simon and E. G. Gwinn, *ACS Nano*, 2014, **8**, 6883–6892.
- J. T. Petty, O. O. Sergev, M. Ganguly, I. J. Rankine, D. M. Chevrier and P. Zhang, *J. Am. Chem. Soc.*, 2016, **138**, 3469–3477.
- 32 J. T. Petty, M. Ganguly, I. J. Rankine, D. M. Chevrier and P. Zhang, *J. Phys. Chem. C*, 2017, **121**, 14936–14945.
- J. T. Petty, M. Ganguly, A. I. Yunus, C. He, P. M. Goodwin, Y. H. Lu and R. M. Dickson, *J. Phys. Chem. C*, 2018, **122**, 28382–28392.
- H. Häkkinen, S. Malola and M. F. Matus, *J. Phys. Chem. C*, DOI:10.1021/acs.jpcc.3c04103.
- 35 S. M. Copp, P. Bogdanov, M. Debord, A. Singh and E. Gwinn, *Adv. Mater.*, 2014, **26**, 5839–5845.
- 36 S. M. Copp, A. Gorovits, S. M. Swasey, S. Gudibandi, P. Bogdanov and E. G. Gwinn, *ACS Nano*, 2018, **12**, 8240–8247.
- 37 S. M. Copp, S. M. Swasey, A. Gorovits, P. Bogdanov and E. G. Gwinn, *Chem. Mater.*, 2020, **32**, 430–437.

- F. Moomtaheen, M. Killeen, J. Oswald, A. Gonzàlez-Rosell, P. Mastracco, A. Gorovits, S. M. Copp and P. Bogdanov, in *Proceedings of the 28th ACM SIGKDD International Conference on Knowledge Discovery & Data Mining*, 2022.
- 39 C. Cerretani, J. Kondo and T. Vosch, *RSC Adv.*, 2020, **10**, 23854–23860.
- 40 C. Cerretani, J. Kondo and T. Vosch, *CrystEngComm*, 2020, **22**, 8136–8141.
- 41 E. Largy, A. König, A. Ghosh, D. Ghosh, S. Benabou, F. Rosu and V. Gabelica, *Chem. Rev.*, 2022, **122**, 7720–7839.
- M. Walter, J. Akola, O. Lopez-Acevedo, P. D. Jadzinsky, G. Calero, C. J. Ackerson, R. L. Whetten, H. Grönbeck and H. Häkkinen, *Proc. Natl. Acad. Sci. U. S. A.*, 2008, **105**, 9157–62.
- 43 R. L. Lundblad, *Handb. Biochem. Mol. Biol.*, 2018, 944–950.
- J. Kypr, I. Kejnovska, D. Renciuk and M. Vorlickova, *Nucleic Acids Res.*, 2009, **37**, 1713–1725.
- 45 D. M. Gray, R. L. Ratliff and M. R. Vaughan, *Methods Enzymol.*, 1992, **211**, 389–406.
- 46 N. V Karimova and C. M. Aikens, *J. Phys. Chem. A*, 2015, **119**, 8163–8173.
- 47 D. J. E. Huard, A. Demissie, D. Kim, D. Lewis, R. M. Dickson, J. T. Petty and R. L. Lieberman, *J. Am. Chem. Soc.*, 2019, **141**, 11465–11470.
- 48 X. Chen, M. Boero and O. Lopez-Acevedo, *Phys. Rev. Mater.*, 2020, 4, 065601.
- 49 I. Dolamic, B. Varnholt and T. Bürgi, *Nat. Commun.*, 2015, **6**, 1–6.
- 50 K. R. Krishnadas, L. Sementa, M. Medves, A. Fortunelli, M. Stener, A. Fürstenberg, G. Longhi and T. Bürgi, *ACS Nano*, 2020, **14**, 9687–9700.
- 51 R. W. Y. Man, H. Yi, S. Malola, S. Takano, T. Tsukuda, H. Häkkinen, M. Nambo and C. M. Crudden, *J. Am. Chem. Soc.*, 2022, **144**, 2056–2061.
- 52 A. Pniakowska, M. Samoć and J. Olesiak-Bańska, *Nanoscale*, 2023, **15**, 8597–8602.
- M. Monti, G. Brancolini, E. Coccia, D. Toffoli, A. Fortunelli, S. Corni, M. Aschi and M. Stener, *J. Phys. Chem. Lett.*, 2023, **14**, 1941–1948.
- 54 Y. Zhu, J. Guo, X. Qiu, S. Zhao and Z. Tang, *Accounts Mater. Res.*, 2021, **2**, 21–35.
- W. D. Si, Y. Z. Li, S. S. Zhang, S. Wang, L. Feng, Z. Y. Gao, C. H. Tung and D. Sun, ACS Nano, 2021, 15, 16019–16029.
- R. Guha, M. Rafik, A. Gonzàlez-Rosell and S. M. Copp, *Chem. Commun.*, DOI:10.1039/D3CC02896H.
- 57 P. R. O'Neill, E. G. Gwinn and D. K. Fygenson, *J. Phys. Chem. C*, 2011, **115**, 24061–24066.